Optics Communications 349 (2015) 83–88

Contents lists available at ScienceDirect

Optics Communications

journal homepage: www.elsevier.com/locate/optcom

A low cost surface plasmon resonance biosensor using a laser line generator

Ruipeng Chen [a], Manping Wang [a], Shun Wang [a], Hao Liang [c], Xinran Hu [d], Xiaohui Sun [a], Juanhua Zhu [a], Liuzheng Ma [a], Min Jiang [e], Jiandong Hu [a,b], Jianwei Li [a,*]

[a] College of Mechanical and Electrical Engineering, Henan Agricultural University, Zhengzhou 450002, China
[b] State Key Laboratory of Wheat and Maize Crop Science, Zhengzhou 45002, China
[c] Department of Electronic and Telecommunications, University of Gavle, Kungsbäcksvägen 47, Gävle 80176, Sweden
[d] School of Human Nutrition and Dietetics, McGill University, Macdonald Campus, 21, 111 Lakeshore Road, Ste Anne de Bellevue, Quebec, Canada H9X 3V9
[e] College of Life Sciences, Henan Agricultural University, Zhengzhou 450002, China

ARTICLE INFO

Article history:
Received 26 November 2014
Received in revised form
2 March 2015
Accepted 17 March 2015
Available online 20 March 2015

Keywords:
Laser line generator
Microprocessor
Biosensor
Surface plasmon resonance
Amplitude-limiting filtering algorithm

ABSTRACT

Due to the instrument designed by using a common surface plasmon resonance biosensor is extremely expensive, we established a portable and cost-effective surface plasmon resonance biosensing system. It is mainly composed of laser line generator, P-polarizer, customized prism, microfluidic cell, and line Charge Coupled Device (CCD) array. Microprocessor PIC24FJ128GA006 with embedded A/D converter, communication interface circuit and photoelectric signal amplifier circuit are used to obtain the weak signals from the biosensing system. Moreover, the line CCD module is checked and optimized on the number of pixels, pixels dimension, output amplifier and the timing diagram. The micro-flow cell is made of stainless steel with a high thermal conductivity, and the microprocessor based Proportional-Integral-Derivative (PID) temperature-controlled algorithm was designed to keep the constant temperature (25 °C) of the sample solutions. Correspondingly, the data algorithms designed especially to this biosensing system including amplitude-limiting filtering algorithm, data normalization and curve plotting were programmed efficiently. To validate the performance of the biosensor, ethanol solution samples at the concentrations of 5%, 7.5%, 10%, 12.5% and 15% in volumetric fractions were used, respectively. The fitting equation $\Delta RU = -752987.265 + 570237.348 \times RI$ with the *R*-Square of 0.97344 was established by delta response units (ΔRUs) to refractive indexes (RI). The maximum relative standard deviation (RSD) of 4.8% was obtained.

1. Introduction

Surface plasmon resonance (SPR) biosensors are designed and widely used in the detection and identification of viruses, hormones and proteins in field such as food safety, biomedical, disease diagnosis and proteomics due to their non-invasive, label-free and on-line dynamic properties of measurement [1–5]. Furthermore, it is a useful and important technology to be studied on biomolecular interactions when one of the two interactants is immobilized onto the sensor surface first, while the other is free in sample solution and also flowed over the sensor surface [6–9]. The processes of the association and dissociation were monitored by and displayed in a response curve in arbitrary unit. A surface plasmon is produced by a p-polarized laser beam which impinges on the interface between the glass (prism) and the metal film (Au film) deposited on the glass surface when the incident angle of the laser beam is larger than the angle of total internal reflection [10–15]. A typical surface plasmon wave propagating along the interface can be realized by the so-called Kretschmann configuration [16–18]. The special angle at which the surface plasmon resonance occurs is extremely sensitive to any changes in the refractive index of the medium adjacent to the metal surface, and such changes can be monitored by recording the intensity of reflected light when the sample solution is flowed through the microfluidic cell [19–21].

Although surface plasmon resonance is a powerful technique to analyze biomolecular interactions in real-time in a label free environment, at present, the cost of the instrument designed by the surface plasmon resonance technology is still extremely expensive due to the complicated configuration of optics and electronics. In practice, the portable and cost-effective surface plasmon

* Corresponding author.
E-mail address: hauljw@163.com (J. Li).

http://dx.doi.org/10.1016/j.optcom.2015.03.035
0030-4018/

resonance instruments are urgently developed and have potential for use in many fields including medicine diagnostics, drug screening and basic scientific research [22–27]. With the ongoing requirements of low cost and portable instruments, we present in this work a portable surface plasmon resonance biosensor for identifying the biomoleculars in sample solutions, which consists of the laser line generator and the line CCD array. In order to reduce the cost of this biosensor, the circuit, that is mainly composed of a line CCD array, a microprocessor PIC24FJ128, and communication interface, should be economically designed. In order to keep the temperature of the microfluidic cell and biosensor constant, the Thermal Electric Chip (TEC) with the control algorithm (PID) is applied and optimized to adjust the current flowing through the TEC according to the atmosphere temperature. A comprehensive optimization analysis on the biosensor designed by using the laser line generator to obtain the performance parameters regarding the dependence of sensitivity on optics and electronics is presented in this work.

2. Materials and methods

2.1. Materials

The laser line generator (dimension ⌀16 mm × 45 mm, wavelength 780 nm, beam divergent angle 65°) was purchased from SFOLT Co., Ltd (Shanghai, China). The high speed acquisition circuit board with line CCD array (UPD3575 module) was purchased from Tianjin Brilliance Photoelectric Technology Co., Ltd. BK7 prism with 50 nm Au film was customized in Changchun Dingxin photoelectric Co., Ltd. The optical adjustment bracket for holding the right angle prism was fabricated in Henan Nongda Xunjie Measurement and Testing Technology Co., Ltd. Ethanol and PBS were purchased from Shanghai General Chemical Reagent Factory (Shanghai, China).

2.2. Setup of the SPR biosensor

The schematic diagram for constructing the surface plasmon resonance biosensor is depicted in Fig. 1. From Fig. 1c, it is known that the evanescent wave produced from the total internal reflection acts on the prism can excite a standing charge density wave on the gold surface [17]. A surface plasmon wave will be produced by the standing charge density at the interface between the metal film and biological medium, which is a P-polarized electromagnetic wave due to P-polarized light being parallel to the incident plane while the S-polarized light being perpendicular to the incident plane.

For the biosensor constructed by a prism with the coupling method of the attenuated total reflection, the propagation constants of the incident light wave and the surface plasmon wave along the *x*-axis will be obtained in the following equations:

$$K_x^{pr} = \sqrt{\epsilon_{pr}}\frac{\omega}{C}\sin\theta_{pr} \tag{1}$$

$$K_x^{sp} = \sqrt{\frac{\tilde{\epsilon}_m \epsilon_s}{\tilde{\epsilon}_m + \epsilon_s}}\frac{\omega}{C} \tag{2}$$

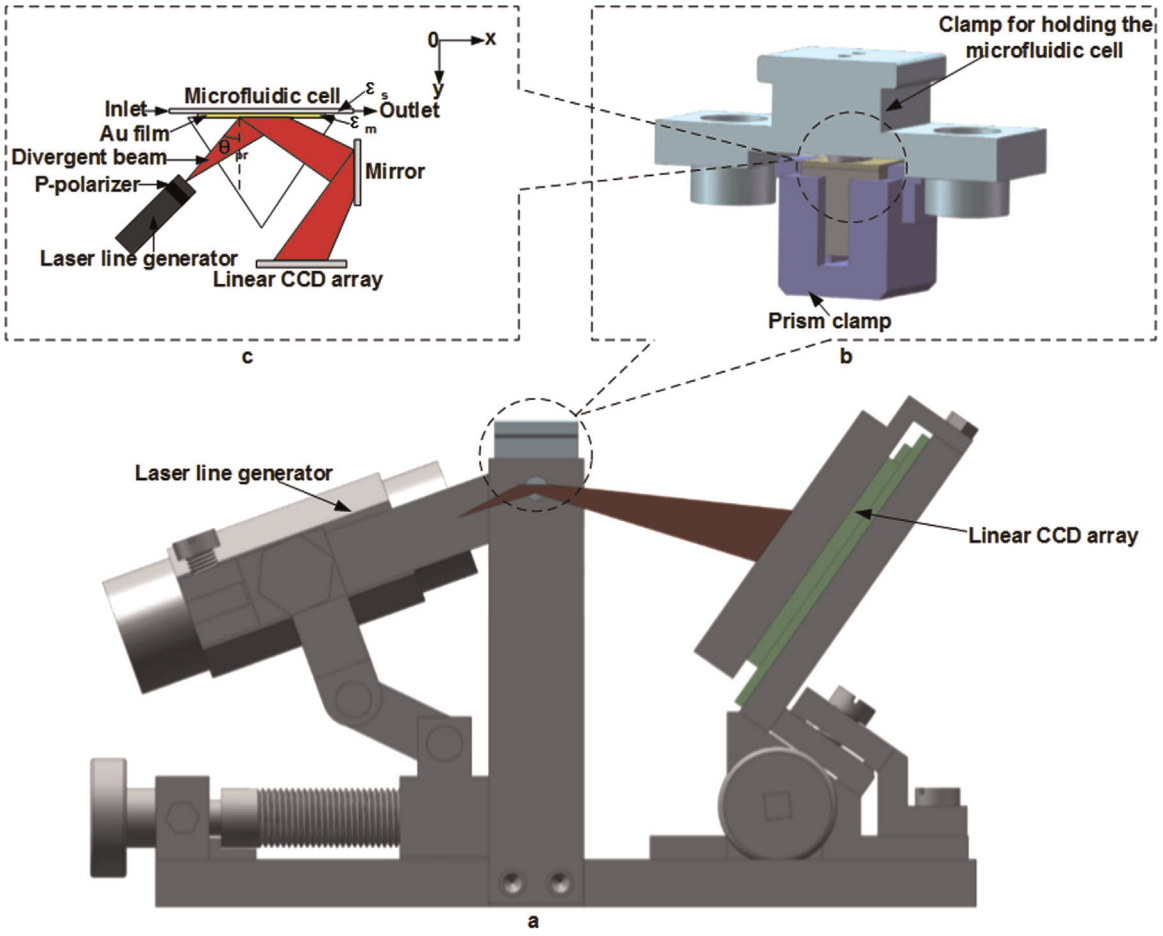

Fig. 1. Schematic of the surface plasmon resonance biosensor using the laser line generator and a linear CCD.

$$K_x^{pr} = \sqrt{\epsilon_{pr}}\frac{\omega}{C}\sin\theta_{pr} = \sqrt{\frac{\tilde{\epsilon}_m \epsilon_s}{\tilde{\epsilon}_m + \epsilon_s}}\frac{\omega}{C} = K_x^{sp} \quad (3)$$

where the propagation constants for incident light wave and the surface plasmon wave are indicated with $K_x{}^{sp}$, $K_x{}^{pr}$, respectively. $\tilde{\epsilon}_m$ is the complex refractive index of the metal film. θ_{pr} is the angle formed between the incident light and the normal line of the prism. ϵ_s is the refractive index of the biological sample flowed through the metal film surface. C is the speed of light and ω is the frequency of the surface plasmon wave.

Both propagation constants will be equal, $K_x^{sp} = K_x^{pr} = K_x$, while the surface plasmon resonance phenomenon occurring. At the resonance point, the intensity of the incident light is absorbed greatly. The intensity of reflective light is approximately zero. By using this relationship, the refractive index of the biological sample bound on the surface of gold film will be calculated. After the light at a certain wavelength and certain angle is shone on the interface between the prism and the Au film, the surface plasmon and the photon inside the Au film will be absorbed. This is seen by a minimum intensity value in the reflection spectra. The position of the minima is indicative of the chemistry on the surface of the SPR sensor. The shift for the minimum value is a measure of the dielectric constant or refractive index changes on the Au surface.

The laser line generator is the key component to be used to excite the free electronics which were oscillated inside the metal film (Au film) originally to produce the surface plasmon. In this setup, the laser line generator does not need to be moved to change the angle of the incident beam which shines on the interface between the end of the prism and the Au film, so that the laser line generator was exactly fixed. The divergent angle of the laser line generator related to the incident beam is totally different from the light source used in the conventional surface plasmon resonance instrument. The microfluidic cell should be embedded in the clamp firstly. Then the incident beam is adjusted to shine on the microfluidic cell attached on the Au film surface of the SPR biosensor. Finally, the position of the linear CCD array was fixed by fine-tuning the knob. The advantages of this biosensor are its components are fixed and the surface plasmon wave is generated by changing the angle of incident light. This extremely reduces the cost of the instrument if an instrument is developed using this platform of biosensor.

The hardware components are combined to realize that the function of this SPR biosensor has been plotted as the block diagram shown in Fig. 2 in terms of the functional requirements of this biosensor. The data obtained from the linear CCD was transmitted to the module of signals condition circuit, which can be used to amplify the photoelectric signals. The properties of the A/D converter used to convert the photoelectric signals into digital signals are intensively studied. The light intensity of the laser line generator can be controlled through the I/O port embedded inside the microprocessor. In the circuit of the surface plasmon resonance biosensor, the microcontroller PIC24FJ128GA006 was utilized to receive the data from the A/D converter, to calculate the pixel positions at the surface plasmon resonance occurring, to plot the surface plasmon resonance curve, and to perform the kinetics analysis.

In order to keep the constant internal temperature of the SPR biosensor platform and the microfluidic cell to improve the signal-noise-ratio (SNR), the special circuit module was designed and constructed technically for the temperature control system. The biosensor module and the microfluidic cell were enclosed in a stainless steel clamp, which was machined for optimal contact with the biosensor module and the temperature controller with a TEC. In this experiment, the stainless steel housing was insulated in an opaque black plastic box for better temperature control and for smaller impact of ambient light. In this experiment, two electric fans are used to disturb the internal wind inside the housed plastic box to adjust the temperature of the TEC chip associating with the atmosphere temperature. The alarm will be triggered if one of the electric fans was damaged. The information of the working status including the internal temperature in Celsius degree and fans speed in revolutions per second (RPS) was transmitted to upper PC and was monitored on the screen in real time.

2.3. CCD circuit

The photoelectronic signals from the line CCD array (UPD3575 module) in this SPR biosensing system were obtained by the

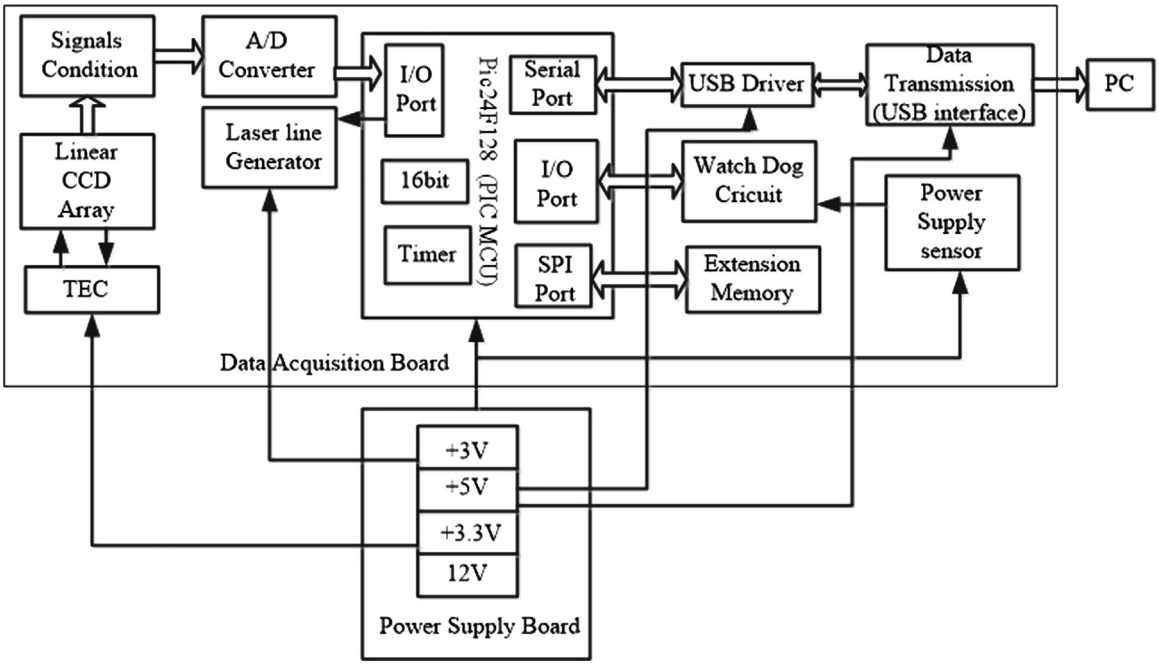

Fig. 2. Functional block diagram of the surface plasmon resonance bioanalyzer.

following approach shown in Fig. 2. The UPD3575D is a 1024-bit photo sensor array.

The main features of this linear CCD module include the built-in driving circuit capable of directly driving TTL loads, the built-in output signal amplifier and sample hold circuit, a single 12 V power source, and the low average dark voltage (less than 0.5 mV). The output voltage (V_{out}) of the pixel signals starts to be changed while the arrival of the falling edge of the pixel synchronizing pulse (PSP) is coming. The V_{out} was kept changing when the pixel synchronizing pulse is low level until the coming of the rising edge of PSP, and the V_{out} will be achieved stably while the PSP becomes high level in the first half cycle. The V_{out} will be decreased up to 0 V while the PSP kept a high level in the second half cycle. Therefore, the A/D converter will be started to run once the pixel synchronizing pulse's rising edge comes in. The sampling process of the A/D converter must be finished in the period of half high level. Otherwise, V_{out} will be dropped. The following conversion will be started automatically after the sampling being ended. Then the results from the A/D converter will be stored in the extensive memory after it was accumulated and averaged by the microcontroller.

2.4. Calculation formulas

2.4.1. RU value

The intensity of response signals (RU, response unit) from the SPR biosensor is calculated by

$$\mathrm{RU} = \frac{D_{Sample,on} - D_{Water,off}}{D_{Air,on} - D_{Air,off}} \times 30000 \tag{4}$$

where $D_{Sample,on}$ is the A/D converted value of the voltage from the line CCD array when the biological sample solution is flowed through the surface of the Au film with the laser on. $D_{Water,off}$ is the A/D converted value of the voltage from CCD when the deionized water is injected through the Au film surface with the laser off. $D_{Air,on}$ is the A/D converted value of the voltage from CCD when the air fully fills in the microfluidic cell with the laser on. $D_{Air,off}$ is the A/D converted value of the voltage from CCD when the surface of the Au film is dry under the laser off. The amplitude-limiting filtering algorithm was used to eliminate the gross errors in processing the A/D converted value from the CCD before calculating the RU. The SPR curve was produced by plotting RU values obtained from the median filter on the *Y*-axis, and the time on the *X*-axis.

2.4.2. Amplitude-limiting filtering algorithm

As the CCD array was used in this experiment, $D_{Sample,on}$, $D_{Sample,off}$, $D_{Air,on}$, and $D_{Air,off}$, define before, obtained from the A/D converter do not obey the statistical law completely. The traditional method for removing gross errors only process data as pure numerical value. It does not reflect the characteristics of data changed with time. Taking amplitude-limiting filtering algorithm into account for processing the raw data, the gross error problem can be solved efficiently. Otherwise, the gross error will affect the value of RUs greatly with reference to the formula (4).

The following procedure for programming is considered. (1) The A/D converted values, such as $D_{Sample,on}$, $D_{Sample,off}$, $D_{Air,on}$, and $D_{Air,off}$, are stored in the RAM in a temporal sequence, which can only be temporary read and restored, and are expressed as X_1, $X_2, X_3, \ldots, X_n$, respectively. The first one of the A/D converted values is X_1, while the last one is X_n. (2) The increment of the two adjacent A/D converted values is denoted as Y_i, namely, $Y_1 = X_2 - X_1$, $Y_2 = X_3 - X_2$, $Y_3 = X_4 - X_3$, …, $Y_i = X_{i+1} - X_i$, …, $Y_{n-1} = X_n - X_{n-1}$. (3) The maximum permissible increment (denoted A) of both adjacent A/D converted values was determined by the maximum slope (denoted V_{max}) of X_i and the sample period *T*. So the *A* value can be calculated by

$$A = KV_{max}\,T \tag{5}$$

where *K* is the constant coefficient. Obviously, the amplitude-limiting filtering algorithm will be understood completely by using the following criteria:

$$\Delta x = |y_i| \begin{cases} \le A, & \bar{x}_i = x_i \\ > A, & \bar{x}_i = \bar{x}_{i-1} \end{cases} \tag{6}$$

where $\bar{x}_i$ is the result from the amplitude-limiting filtering algorithm in the *i*th sampling period. x_i is the sampling value in corresponding *i*th sampling period without amplitude-limiting filtering, while $\bar{x}_{i-1}$ is the previous value obtained from the amplitude-limiting filter.

3. Results and analysis

3.1. Temperature experiments

Changes in temperature will cause significant changes in the refractive index of aqueous solution, which will affect SPR signals. [28] The thermoelectric cooler (TEC semiconductor chip) is the key component used in this experiment for heating or cooling by changing the current direction through the TEC chip. The driver with the PID algorithm was designed to control the internal temperature of the biosensor for keeping it working at the temperature of 25 °C. The narrow measurement range of temperature was obtained by a thermistor sensor to improve the precision of the constant temperature controller. A 16-bit A/D converter was utilized in the temperature control circuit, which was set to work at a differential mode (both input voltages change in opposite directions). The resolution of the ADS 0832 is equivalent to the ADC working at 15-bit due to one sign bit used. Hence, the A/D converted values were changed in the range from 0 to 32 767. The temperature range which can be measured by the thermistor sensor should be as small as possible to obtain the resolution of 0.01 °C. For example, the A/D converter value of 327 was gotten with the variation of 1 °C in the temperature measurement range from 0 to 100 °C, and so on. The A/D converted value of approximately 3 was gotten with the variation of 0.01 °C in the same temperature range of 100 °C. It can be apparent that the narrower the temperature measurement range, the larger the A/D converted value at the variation of 0.01 °C can be obtained. Obviously, the high-precision temperature controller was designed in the temperature measurement range from 0 to 2 °C. In this situation, the A/D converted value of 16 383 was gotten with the variation of 1 °C in the temperature measurement range of 2 °C, while the A/D converted value of 163 was gotten with the variation of 0.01 °C in the same temperature measurement range of 2 °C.

In order to validate the properties of this temperature controller, the disturbance suppressing characteristics are needed to verify accordingly. It was defined as that the temperature control system can adjust the temperature automatically to reach the constant temperature point regardless the disturbances of the outside temperature. The time needed to achieve the constant temperature point is the key parameter that should be concerned about in this issue. In this experiment, the current flowed through to the TEC chip for heating was cut off if the temperature deviation is larger than the A/D converted value of 16 000 (corresponding to 1 °C). However, the cooling system starts to work then.

After the temperature perturbation was stopped, the time-dependent temperature changes of the temperature control system using TEC chip was shown in Fig. 3. In the beginning of the time, a

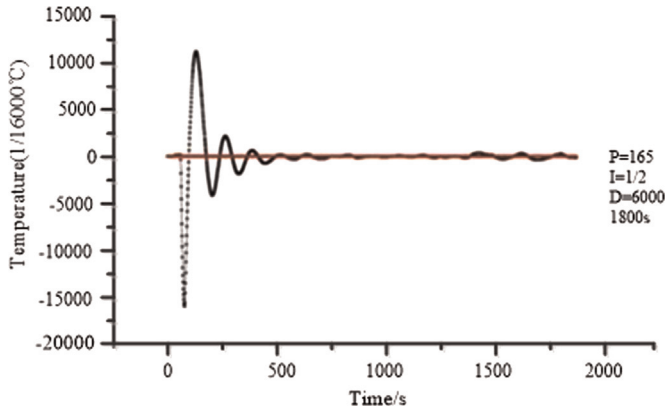

Fig. 3. The time-dependent temperature changes of the temperature controlling system.

big peek occurs during this time. Then the temperature value drops rapidly to reach the steady state after working for 500 s under the parameters of $P=165$, $I=0.5$ and $D=6000$.

3.2. SPR curve

RU is derived from the refractive index of the medium adjacent to the Au film surface of the biosensor. The refractive index of a prepared ethanol solution sample is dependent on the volumetric faction (indicated with v/v ratio). Hence, the value of RU may be varied with different sample concentrations.

By taking the ethanol solution as the standard detected sample, no ligand was immobilized on the biosensor surface where 50 nm gold film was deposited as the specific acceptor for identifying the ethanol molecules to avoid influencing produced by the biomolecular identification membrane [29]. The several known concentrations of the ethanol solutions are 5%, 7.5%, 10%, 12.5% and 15% in volumetric fractions, respectively and the deionized water was flowed successively over the biosensor surface to obtain the baseline signals. The response signals obtained from the different concentrations were shown in Fig. 4. The SPR curve became smooth due to the PID temperature algorithm.

There are distinct differences between the two curves obtained from two adjacent sample concentrations, which demonstrated that a higher sensitivity can be achieved.

The background of 3000 shown in Fig. 4 was automatically set by the operating software. A normal calibration method was

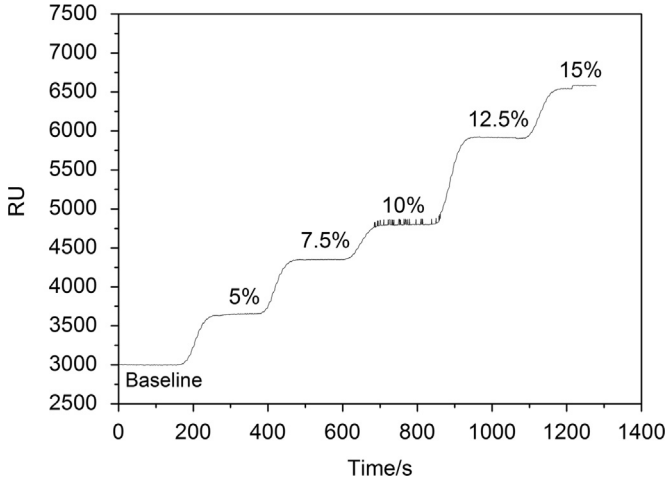

Fig. 4. Sensor response diagram obtained from different concentrations of ethanol solutions. The sensorgram obtained from known concentrations of 5%, 7.5%, 10%, 12.5% and 15% in volumetric fractions, respectively.

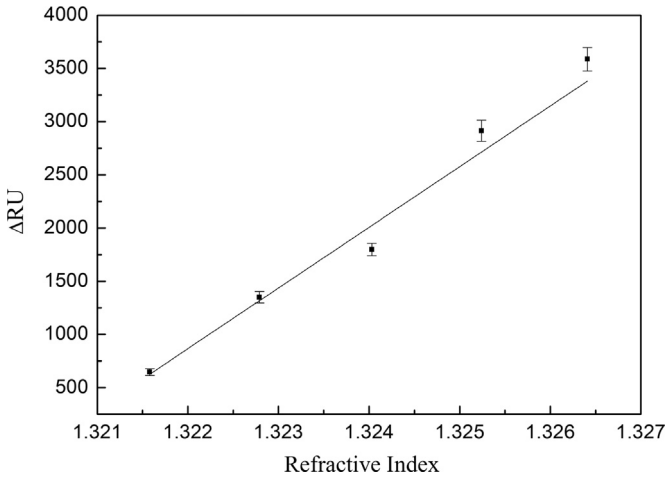

Fig. 5. The fitting curve established by delta response units with different refractive indexes.

applied to convert the RU values which was obtained from the deionized water flowed through the Au film surface of the SPR biosensor. After that, the resolution was improved by avoiding the calculation of the very small number.

In order to determine the effectiveness of this biosensing platform designed by using the laser line generator, the ethanol solution samples with concentrations of 5%, 7.5%, 10%, 12.5% and 15% were measured repeatedly for five times, respectively. The mean response values of these known concentration samples were calculated to be 647, 1349, 1798, 2194, 3586 in delta response units (ΔRU), which reflect the biosensor sensor response induced by analyte binding that change the local reflective index (RI) at the biosensor sensor interface. Importantly, a background response will also be generated if there is a difference in the refractive indexes of the running and sample buffers. This background response must be subtracted from the sensorgram to obtain the actual binding response. Hence the refractive index of the medium is directly related to the ΔRU. In Fig. 5, the fitting equation $\Delta RU = -752987.265 + 570237.348 \times RI$, where RI is the refractive index of the ethanol solution sample, can be obtained with the *R*-Square of 0.97344. The mean and the standard deviation (SD) obtained from each ethanol sample solution are shown with error bar in Fig. 5. It showed that the response relationship to the different ethanol solution samples is very satisfactory despite the variation occurred in the single-time measurement.

4. Conclusions

The circuit and data processing designed for this SPR platform using the laser line generator have been presented. It is capable of detecting chemical and biological substances. The circuit for collecting the signals from the linear CCD array and transferring measurement results to the computer is mainly composed of a microprocessor PIC24FJ128GA006, a driver circuit for running the laser line generator, a watchdog circuit for monitoring the power supply, an extension memory for storing the initialized parameters and measurement results, and a temperature controller chip (TEC). The amplitude-limiting filter and the median filter have been programmed and analyzed. The UPD3575D CCD module with a 1024 bit linear image sensor capable of converting light into voltage has chosen and the integration time and the pixel synchronizing pulse's cycle have been intensively discussed. In order to keep the constant temperature of the surface plasmon resonance biosensor constant, the TEC with PID algorithm is utilized. In this

experiment, a 16-bit A/D converter ADC0832 was used in the temperature control circuit, which was initialized to work at the differential mode to reach the temperature of 25 °C with the small deviation of ± 0.5 °C.

To validate the performance of the biosensor, ethanol solution samples at the concentrations of 5%, 7.5%, 10%, 12.5% and 15% in volumetric fractions were used, respectively. The fitting equation $\Delta RU = -752987.265 + 570237.348 \times RI$ with the *R*-Square of 0.97344 was established by delta response units (ΔRUs) to refractive indexes (RI). The maximum relative standard deviation (RSD) of 4.8% was obtained. Changes in refractive indexes of biological analytes adjacent to the Au film surface of the biosensor can be detected by this SPR biosensor. Therefore, this biosensor can be used in the detection of association and dissociation rate of biomolecular interactions.

Future work will involve the continuation of laboratory tests as well as field trials to obtain more data of high sensitivity and reliability for this biosensing system with the optimization of the algorithm for obtaining the precise position of the resonant dip and the optimization of the circuit design with microprocessors.

Conflicts of Interest

The authors declare no conflict of interest.

Author contributions

In this work, the general conception has been developed by Manping Wang, Hao Liang, Jiandong Hu and Jianwei Li, while the amplitude-limiting filtering algorithm has been developed by Hao Liang and Ruipeng Chen. Moreover, Xinran Hu has prepared the draft manuscript and Ruipeng Chen, Hao Liang, Xiaohui Sun and Jianwei Li have designed the circuit. Shun Wang, Juanhua Zhu and Min Jiang have performed the experiments. Liuzheng Ma contributed in the figures.

Acknowledgments

This research was supported by State Key Laboratory of Wheat and Maize Crop Science, and also supported by Henan province joint funding program, Grant no. U1304305 of the National Natural Science Foundation of China.

References

[1] M. Piliarik, L. Párová, J. Homola, High-throughput spr sensor for food safety, Biosens. Bioelectron. 24 (2009) 1399–1404. http://dx.doi.org/10.1016/j.bios.2008.08.012.

[2] H. Vaisocherová, V.M. Faca, A. Taylor, S. Hanash, S. Jiang, Comparative study of spr and elisa methods based on analysis of cd166/alcam levels in cancer and control human sera, Biosens. Bioelectron. 24 (2009) 2143–2148. http://dx.doi.org/10.1016/j.bios.2008.11.015.

[3] D. Enrico, M. Manera, G. Montagna, F. Cimaglia, M. Chiesa, P. Poltronieri, A. Santino, R. Rella, Spr based immunosensor for detection of legionella pneumophila in water samples, Opt. Commun. 294 (2013) 420–426. http://dx.doi.org/10.1016/j.optcom.2012.12.064.

[4] J. Homola, Present and future of surface plasmon resonance biosensors, Anal. Bioanal. Chem. 377 (2003) 528–539. http://dx.doi.org/10.1007/s00216-003-2101-0.

[5] M. Piliarik, H. Vaisocherová, J. Homola, Surface plasmon resonance biosensing, Methods Mol. Biol. 503 (2009) 65–88. http://dx.doi.org/10.1007/978-1-60327-567-5_5.

[6] T. Xue, X. Cui, W. Guan, Q. Wang, C. Liu, H. Wang, K. Qi, D. Singh, W. Zheng, Surface plasmon resonance technique for directly probing the interaction of dna and graphene oxide and ultra-sensitive biosensing, Biosens. Bioelectron. 58 (2014) 374–379. http://dx.doi.org/10.1016/j.bios.2014.03.002.

[7] S. Patching, Surface plasmon resonance spectroscopy for characterisation of membrane proteinligand interactions and its potential for drug discovery, Biochim. Biophys. Acta 1838 (2014) 43–55. http://dx.doi.org/10.1016/j.bbamem.2013.04.028.

[8] B. Bécsi, A. Kiss, F. Erd, Interaction of protein phosphatase inhibitors with membrane lipids assessed by surface plasmon resonance based binding technique, Chem. Phys. Lipids 183 (2014) 68–76. http://dx.doi.org/10.1016/j.chemphyslip.2014.05.009.

[9] P. Sandblad, R. Arnell, J. Samuelsson, T. Fornstedt, Approach for reliable evaluation of drug proteins interactions using surface plasmon resonance technology, Anal. Chem. 81 (2009) 3551–3559. http://dx.doi.org/10.1021/ac900299p.

[10] Y. Shin, H. Kim, Y. Jung, B. Chung, A new palm-sized surface plasmon resonance (spr) biosensor based on modulation of a light source by a rotating mirror, Sens. Actuators B 150 (2010) 1–6. http://dx.doi.org/10.1016/j.snb.2010.08.006.

[11] H. Ho, W. Law, S. Wu, X. Liu, S. Wong, C. Lin, S. Kong, Phase-sensitive surface plasmon resonance biosensor using the photoelastic modulation technique, Sens. Actuators B 114 (2006) 80–84. http://dx.doi.org/10.1016/j.snb.2005.04.007.

[12] K.M.N. Shankaran, D.R. Gobi, Recent advancements in surface plasmon resonance immunosensors for detection of small molecules of biomedical, food and environmental interest, Sens. Actuators B 121 (2007) 158–177.

[13] P. Novo, V. Chu, J. Conde, Integrated optical detection of autonomous capillary microfluidic immunoassays: a hand-held point-of-care prototype, Biosens. Bioelectron. 57 (2014) 284–291. http://dx.doi.org/10.1016/j.bios.2014.02.009.

[14] S. Scarano, M. Mascini, A. Turner, M. Minunni, Surface plasmon resonance imaging for affinity-based biosensors, Biosens. Bioelectron. 25 (2010) 957–966. http://dx.doi.org/10.1016/j.bios.2009.08.039.

[15] H. Daghestani, B. Day, Theory and applications of surface plasmon resonance, resonant mirror, resonant waveguide grating, and dual polarization interferometry biosensors, Sensors 10 (2010) 9630–9646. http://dx.doi.org/10.3390/s101109630.

[16] M. Faryad, A. Lakhtakia, On multiple surface-plasmon-polariton waves guided by the interface of a metal film and a rugate filter in the Kretschmann configuration, Opt. Commun. 284 (2011) 5678–5687. http://dx.doi.org/10.1016/j.optcom.2011.08.055.

[17] A. Suzuki, J. Kondoh, Y. Matsui, S. Shiokawa, K. Suzuki, Development of novel optical waveguide surface plasmon resonance (spr) sensor with dual light emitting diodes, Sens. Actuators B 106 (2005) 383–387. http://dx.doi.org/10.1016/j.snb.2004.08.021.

[18] A. Abbas, M. Linman, Q. Cheng, Sensitivity comparison of surface plasmon resonance and plasmon-waveguide resonance biosensors, Sens. Actuators B 156 (2011) 169–175. http://dx.doi.org/10.1016/j.snb.2011.04.008.

[19] A. Abbas, M. Linman, Q. Cheng, New trends in instrumental design for surface plasmon resonance-based biosensors, Biosens. Bioelectron. 26 (2011) 1815–1824. http://dx.doi.org/10.1016/j.bios.2010.09.030.

[20] S. Wu, H. Ho, W. Law, C. Lin, S. Kong, Highly sensitive differential phase-sensitive surface plasmon resonance biosensor based on the Mach–Zehnder configuration, Opt. Lett. 29 (2004) 2378–2380. http://dx.doi.org/10.1364/OL.29.002378.

[21] A. Abbas, M. Linman, Q. Cheng, Patterned resonance plasmonic microarrays for high-performance spr imaging, Anal. Chem. 83 (2011) 3147–3152. http://dx.doi.org/10.1021/ac200190b.

[22] D. Jang, D. Lim, G. Chae, J. Yoo, A novel algorithm based on the coefficient of determination of linear regression fitting to automatically find the optimum angle for miniaturized surface plasmon resonance measurement, Sens. Actuators B 199 (2014) 488–492. http://dx.doi.org/10.1016/j.snb.2014.03.103.

[23] S. Kima, K. Gobib, H. Iwasakac, H. Tanaka, N. Miura, Novel miniature spr immunosensor equipped with all-in-one multi-microchannel sensor chip for detecting low-molecular-weight analytes, Biosens. Bioelectron. 23 (2007) 701–707. http://dx.doi.org/10.1016/j.bios.2007.08.010.

[24] A. Hemmi, T. Imato, Y. Aoki, M. Sato, N. Soh, Y. Asano, C. Akasaka, S. Okutani, S. Ohkubo, N. Kaneki, K. Shimada, T. Eguchi, T. Oinuma, Development of palm-sized differential plasmon resonance meter based on concept of sprode, Sens. Actuators B 108 (2005) 893–898. http://dx.doi.org/10.1016/j.snb.2004.12.103.

[25] S. Roh, T. Chung, B. Lee, Overview of the characteristics of micro- and nano-structured surface plasmon resonance sensors, Sensors 11 (2011) 1565–1588. http://dx.doi.org/10.3390/s110201565.

[26] A. Karabchevsky, S. Karabchevsky, I. Abdulhalim, Fast surface plasmon resonance imaging sensor using radon transform, Sens. Actuators B 155 (2011) 361–365. http://dx.doi.org/10.1016/j.snb.2010.12.012.

[27] A. Karabchevsky, L. Tsapovsky, R. Marks, I. Abdulhalim, Study of immobilization procedure on silver nanolayers and detection of estrone with diverged beam surface plasmon resonance (spr) imaging, Biosensors 3 (2013) 157–170. http://dx.doi.org/10.3390/bios3010157.

[28] A. Naimushin, S. Soelberg, D. Bartholomew, J. Elkind, C. Furlong, A portable surface plasmon resonance (spr) sensor system with temperature regulation, Sens. Actuators B 96 (2003) 253–260. http://dx.doi.org/10.1016/S0925-4005(03)00533-1.

[29] Y.-B.S.H.K.Y. Jung, B. Chung, A new palm-sized surface plasmon resonance (spr) biosensor based on modulation of a light source by a rotating mirror, Sens. Actuators B 150 (2010) 1–6. http://dx.doi.org/10.1016/j.snb.2010.08.006.